JOURNAL OF Applied Polymer SCIENCE

Effect of Nanoclay Content and Matrix Composition on Properties and Stress–Strain Behavior of NR/EPDM Nanocomposites

Abdolmajid Alipour,[1] Ghasem Naderi,[2] Mir HamidReza Ghoreishy[2]

[1]Young Researchers Club, Zarghan Branch, Islamic Azad University, Zarghan, Iran

[2]Department of Rubber, Iran Polymer and Petrochemical Institute, Tehran, Iran

Correspondence to: A. Alipour (E-mail: Abdolmajid.Alipoor@gmail.com)

ABSTRACT: Nanocomposites based on NR/EPDM/Cloisite 15A have been prepared via a vulcanization process to investigate the effect of nanoclay content and rubber composition on the properties of samples. The prepared nanocomposite samples are characterized by several techniques. The experimental results of X-ray diffraction and transmission electron microscopy showed the widening of distance between the silicate layers, penetration of polymer chains into silicate layers, and formation of an intercalated and partially exfoliated structure. Results indicated that addition of nanoclay could improve the mechanical strength of the rubber. Also increase of nanoclay and EPDM content were found to improve the thermal aging of the samples and also the performance of the rubbers under compression. Nanoclay also reduced the hysteresis and heat build up of the rubber compounds. Moreover, to investigate the stress–strain behavior of NR/EPDM nanocomposites using constitutive models, applicability and best fit of five different hyperelastic constitutive models including second order Polynominal, Yeoh, third order Ogden, Marlow, and Arruda-Boyce against experimental data for NR/EPDM/nanoclay blends were studied. Due to the different amounts of nanoclay (1, 3, 5, and 7 wt %) and different NR/EPDM compositions (100/0), (75/25), (50/50), (25/75), and (0/100), different experimentally measured data of samples were compared with those predicted by the mathematical models previously mentioned. Results showed that third order Ogden and Marlow models can be used for different amounts of nanoclay and rubber compositions, whereas Arruda-Boyce and Yeoh models show more deviation from experimental data with a reduction in nanoclay and increase in EPDM content. © 2012 Wiley Periodicals, Inc. J. Appl. Polym. Sci. 000: 000–000, 2012

KEYWORDS: clay; nanocomposites; rubber

Received 14 September 2011; accepted 20 March 2012; published online
DOI: 10.1002/app.37752

INTRODUCTION

The blending of two rubbers is a useful method to improve certain properties, which are not inherent in a single rubber. The properties of any blend are functions of the adhesion between the components. While most of the blends are thermodynamically incompatible, many have been found to have technological importance.[1] Natural rubber (NR) can exhibit crystallization when stretched. Stress-induced crystallization can be used to increase modulus and resistance to deformation, preventing the propagation of defects. However, ethylene propylene diene monomer (EPDM) rubber has saturated hydrocarbon backbones, which impart usually good weathering oxidation and chemical resistance.[2,3] The blending of EPDM with NR and other diene rubbers has given rise to compounds with good ozone and chemical resistance and reduced compression set.[4] More recently, polymers containing dispersion of nanometer size (1–100 nm) particles have been studied.[4–9] Among the different nanoparticles, clay has attracted significant attention because it provides two distinct opportunities of processing polymer nanocomposites through intercalation and exfoliation. In an intercalated nanocomposite, the polymer penetrates between the galleries of the clay layers, whereas in exfoliation, the clay layers are completely delaminated and dispersed individually in the polymer matrix. A number of studies have proven that polymer nanocomposites exhibit increase in strength, modulus, flame retardancy, and heat distortion temperature that are not possessed by the individual phases or conventional composites containing micrometer size particles or fibers.

Elastomers are known for their ability to be stretched easily to high extensions and then rapidly reverse back to shape when the stress is released. The major constituents of a typical elastomer compound are long chain molecules known as the base

Table I. Material Characteristics Used in This Work

Material	Characteristics		Units
NR	Mooney viscosity ML (1 + 4)100°C	55	M
	Density	0.913	g/cm^3
EPDM	Mooney viscosity ML (1 + 4)125°C	60	M
	Ethylen content	68	%
	Termonomer content	4.5	% ENB
	Density	0.86	g/cm^3
Cloisite 15A	CEC	125	meq/100g
	Density	1.66	g/cm^3

polymer, which provide the basic chemical and physical characteristics. A small amount of free space (termed "free volume") exists between the long chain molecules. This allows for the movement of the molecules more or less independently of one another. It is this characteristic that allows elastomeric components to deform and change shape. Crosslinks formed within the closely packed molecular network during the vulcanizing or curing process and addition of fillers influence the reversibility of elastomers. Due to properties of elasticity and resilience of rubber materials, rubber has become one of the most important elastomeric material for vibration, isolation, and shock absorption; and more specifically, it is a key component of many load-bearing and vibration-isolation mountings and elastomeric load-bearing structures. In the automotive industry, the widespread use of rubber components for noise and vibration isolation makes it highly desirable to predict rubber component response. Since that the behavior of rubber materials deviates from the linear elastic state, using a single constitutive model for extensive range of rubbers is not possible. Some investigators have studied the use of hyperelastic models for rubber compounds.[10–21] For example, Ghasemi et al.[21] by using four hayperelastic models could find a relationship between morphology and degree of fitting of hyperelastic models for SBR nanocomposites, but to our knowledge no study has been published on the stress–strain behavior of NR/EPDM nanocomposites using hyperelastic models. In this work, we have tried to find a relationship between matrix composition, nanoclay loading, and degree of fitting for the NR/EPDM/Cloisite 15A nanocomposites. So, the hyperelasticity of rubber-like material is first summarized. After investigation of XRD and TEM results of nanocomposite samples, properties of samples are studied. Finally, the effect of clay loading and rubber composition on the applicability of five material models including second order Polynominal, Yeoh, third order Ogden, Marlow, and Arruda-Boyce is investigated.

EXPERIMENTAL

Material

Natural rubber (SMR20), EPDM (KEP 270), nanoclay, and the curing system (Zinc Oxide, Sulfur, Stearic Acid, MBTS, and TBBS) were supplied by Malaysia, Korea Kumho Polychem, Southern clay and Bayer Co., respectively. The nanoclay used was Cloisite 15A which was a natural montmorillonite modified with a dimethyl dehydrogenated tallow quaternary ammonium having a cation exchange capacity of 125 mequiv/100 g. Table I shows the detailed characteristics of the material used here.

Table II. Composition (wt %) and Nomenclature of the Samples Prepared in This Study

Sample ingredient	S_0	S_1	S_2	S_3	S_4	S_5	S_6	S_7	S_8
NR	75	75	75	75	75	100	50	25	0
EPDM	25	25	25	25	25	0	50	75	100
Nanoclay	0	1	3	5	7	3	3	3	3

Sample Preparation

Nanocomposite samples, after predrying of clay at 80°C for 24 h, were prepared by a 2 kg Polymix 200 L two-roll mill for 20 min at room temperature, according to the compositions summarized in Table II. It should be mentioned that NR, clay powder, and EPDM were mixed and then curing system was added to the compound. Curing process was carried out under a Dieffenbacher hot press at 160°C and 150 bar. The vulcanization ingredients including sulfur, mercapto-accelerators (MBTS and TBBS) are summarized in Table III.

Characterization

X-ray diffraction patterns of the samples were recorded on a Philips model X'Pert (50 kV, 40 mA) by using Cu Kα radiation ($\lambda = 1.540598$ Å) with a scanning rate 2°/min at room temperature. The basal spacing of silicates was estimated from the position of the plane peak in the WAXD intensity profile using the Bragg's law, $d = \lambda/(2\sin\theta_{max})$. The nanostructure of the clay was observed by a transmission electron microscopy (TEM) (JEM-2100F, JEOL) of cryogenically microtomed (with a diamond knife at −100°C) fracture surface of the samples with a voltage accelerator of 200 kV. Tensile strength and compression strength of samples were carried out according to ASTM D 412 and ISO 7743, respectively, by a Hiwa machine (Iran). For Accelerated Thermal Aging Test, the rubber samples were subjected to accelerated thermal aging in an air circulated oven at 90°C for periods of 96 h according to ASTM D573-88. Compression Set results for a material are expressed as percentage. The lower the percentage figure, the better the material resists permanent deformation under a given deflection and temperature range. The specimens are compressed by 50% at 100°C for 24 h. The heat build up of each sample was measured on a Goodrich flexometer at 35 Hz again under standard ISO conditions. The heat index was measured as the ratio between the Goodrich HBU and the hardness IRHD. The amount of toluene absorbed into the NR/EPDM rubber composites was measured,

Table III. The Vulcanization Ingredients

Ingredients	phr
Zinc oxide	5
Stearic acid	2
Sulfur	1.5
N-tertiarybutyl-2-benzothiazole sulfonamide (TBBS)	1.5
Benzothiazyl disulfide (MBTS)	0.5

to evaluate the degree of crosslinking. Cured test pieces of dimensions 13 mm × 10 mm × 1.5 mm were weighed. Each test piece was immersed in a glass vessel containing 50 cm^3 of toluene. After 100 h at room temperature, the toluene from the surface of each sample was blotted, and the rubber samples were weighed. The deswollen weight of the samples was measured after drying in a vacuum oven for 24 h.

$$\text{Swelling } \% = \frac{(W_{\text{swollen}} - W_{\text{deswollen}})}{W_{\text{deswollen}}} \times 100 \quad (1)$$

$$\text{Soluble } \% = \frac{(W_{\text{original}} - W_{\text{deswollen}})}{W_{\text{original}}} \times 100 \quad (2)$$

(W_{original} = weight before immersion; W_{swollen} = weight after immersion; $W_{\text{deswollen}}$ = weight after drying).

Introductory Summary of Theoretical Models

Hyperelastic materials are described in relation between strain energy density (SED) stored in the material and three invariants of the strain tensor (I_1, I_2, and I_3).[21–23]

$$\begin{aligned} I_1 &= \lambda_1^2 + \lambda_2^2 + \lambda_3^2 \\ I_2 &= \lambda_1^2\lambda_2^2 + \lambda_2^2\lambda_3^2 + \lambda_1^2\lambda_3^2 \\ I_3 &= \lambda_1^2\lambda_2^2\lambda_3^2 \end{aligned} \quad (3)$$

where $I_3 = 1$ for a perfect incompressible material and λ_1, λ_2, and λ_3 are the three principal stretch ratios. In this investigation, five material models have been recommended to depict nonlinear elastic behavior of nanocomposite samples.

Arruda-Boyce. This model represents the underlying molecular structure of the rubbers to simulate the non-Gaussian behavior of individual chains in the network.[21,23] The form of the Arruda-Boyce strain energy potential is as follows:

$$W = \mu \sum_{i=1}^{5} \frac{C_i}{\lambda_m^{2i-2}} (I_1^i - 3^i) \quad (4)$$

where

$$C_1 = \frac{1}{2}, C_2 = \frac{1}{20}, C_3 = \frac{11}{1050}, C_4 = \frac{19}{7000}, C_5 = \frac{519}{673,750} \quad (5)$$

$$\mu_0 = \mu\left(1 + \frac{3}{5\lambda_m^2} + \frac{99}{175\lambda_m^4} + \frac{513}{875\lambda_m^6} + \frac{12,039}{67,375\lambda_m^8}\right) \quad (6)$$

where W is the strain energy per unit of reference volume and μ_0 is the initial shear modulus.

Marlow. The Marlow model does not contain any explicit relation between strain energy density and/or invariants or stretch ratios. It is assumed that the strain energy density is only a function of the first invariant of the strain tensor, i.e.,

$$W = W(I_1) \quad (7)$$

Since for incompressible material, $I_3 = 0$, so I_1 can be written as follows:

$$I_1 = \lambda_1^2 + \lambda_2^2 + \frac{1}{\lambda_1^2\lambda_2^2} \quad (8)$$

It can be shown that the minimum and maximum values of the I_1 are between 3 and $+\infty$, respectively. The uniaxial form of I_1 from Eq. (8) ($\lambda_2 = 1/(\lambda_1)^{0.5}$) can be written as follows:

$$I_1 = \lambda^2 + \frac{2}{\lambda} \quad (9)$$

It is worth noting that the variation of I_1 in Eq. (9) is also between 3 and $+\infty$. Therefore, it can be concluded that the uniaxial tension test data can be used for the determination of the corresponding strain energy density. To achieve this goal, I_1 in a general 3D problem is first calculated and then the associated value of the λ is determined from Eq. (9). Having computed λ, the stress from the experimental data of a uniaxial tension test is determined and the strain energy density is then calculated by the following:

$$W(I) = \int_0^{\lambda(I)-1} \sigma(\varepsilon) d\varepsilon \quad (10)$$

ε and σ are the nominal strain and stress in uniaxial tension test, respectively, that are directly substituted in Eq. (10). It should be noted that the full incompressibility is assumed, meaning all hyperelastic equations only contain the deviatoric part and the volumetric part is neglected.[21–23]

Ogden. Ogden proposed the strain density function can be described directly in terms of principal stretch ratios as follows:

$$W = \sum_{i=1}^{N} \frac{2\mu_i}{\alpha_i^2} (\lambda_1^{\alpha_i} + \lambda_2^{\alpha_i} + \lambda_3^{\alpha_i} - 3) \quad (11)$$

where μ_i and α_i are material constants.[21–23] In this work, it is assumed that $N = 3$. The initial shear modulus of the rubber in this model is computed by the following:

$$\mu_0 = \sum_{i=1}^{n} \mu_i \quad (12)$$

Polynomial. The general form of a polynomial model is given as follows:

$$W = \sum_{i=0}^{m} \sum_{j=0}^{n} C_{ij} (I_1 - 3)^i (I_2 - 3)^j \quad (13)$$

where C_{ij} is the material constant.[21–23] In this work, it is assumed that $m = n = 2$. Thus, it is expressed by the following form:

$$\begin{aligned} W = {} & C_{10}(I_1 - 3) + C_{01}(I_2 - 3) + C_{11}(I_1 - 3)(I_2 - 3) \\ & + C_{02}(I_2 - 3)^3 + C_{20}(I_1 - 3)^2 + C_{00} + C_{12}(I_1 - 3)(I_2 - 3)^2 \\ & + C_{12}(I_1 - 3)^2(I_2 - 3) + C_{22}(I_1 - 3)^2(I_2 - 3)^2 \end{aligned} \quad (14)$$

Yeoh. This is a special form of the reduced polynomial models in Eq. (13) in which $m = 3$.[22,23]

$$W = C_{10}(I_1 - 3) + C_{20}(I_1 - 3)^2 + C_{30}(I_1 - 3)^3 \quad (15)$$

Fitting Procedure

At the first step, test data were used to characterize the material parameters of the hyperelastic models. As we know, the first deviatoric strain invariant defined as follows:

$$I_1 = \lambda^2 + 2/\lambda \quad (16)$$

which λ is the principal stretch and defined as follows:

$$\lambda = 1 + \varepsilon \quad (17)$$

which ε is nominal strain. Using the Eq. (16) in the strain energy potential equations of each model [eqs. (4), (10), (11), (14), and (15)] and having substituted I_1 by $\left(\lambda^2 + \frac{2}{\lambda}\right)$, the new form of strain energy function for each model can be rewritten. Since the value of force is resulted from (dW/dl) and considering that:

$$\lambda = l/l_0 \quad (18)$$

then we can have:

$$F = V(dW/dl) = V(dW/d\lambda)(d\lambda/dl) = (V/l_0)(dW/d\lambda) \quad (19)$$

which V is the sample volume. Since initial area is: $A_0 = V/l_0$, then the value of nominal stress (F/A_0) (which F is Force) is obtained as follows:

$$\sigma_n = (dw/d\lambda) \quad (20)$$

So, by computing the $(dW/d\lambda)$ in the new form of strain energy function of each model, we can rewrite strain energy function of each model. Now by substituting the ε from the equation $(\lambda = 1 + \varepsilon)$ by λ and having the value of nominal stress, we can get the material parameters of the hyperelastic models as well as the nominal stress as a function of nominal strain curve by curve fitting and using least square fit. It should be noted that the ABAQUS code was used for this purpose.[24]

RESULTS AND DISCUSSION

X-ray Diffraction

XRD is a powerful technique to follow the intercalation of elastomer chains into the silicate layers of clay and dispersion of organoclay in the polymer matrix. Figure 1(a) shows the XRD patterns of NR75/EPDM25/clay nanocomposite samples. The interlayer spacing of the original Cloisite 15A is ($2\theta = 2.9$; $d_{001} = 31.5$Å). Shift of the organoclay diffraction peak to lower 2θ values indicated that elastomer chains intercalated between consequent silicate layers. This clearly indicates that interlamellar spacing of the clay are enlarged after melt compounding. As expected intensity increases with an increase in nanoclay. The decrease in intensity and the broadening of peaks indicate that the stacks of layered silicates become more intercalated or partially exfoliated.[6] Figure 1(b) shows XRD patterns of the different compositions of NR/EPDM blends containing 3 wt % nanoclay. As seen, increase of EPDM content leads to a leftward shift

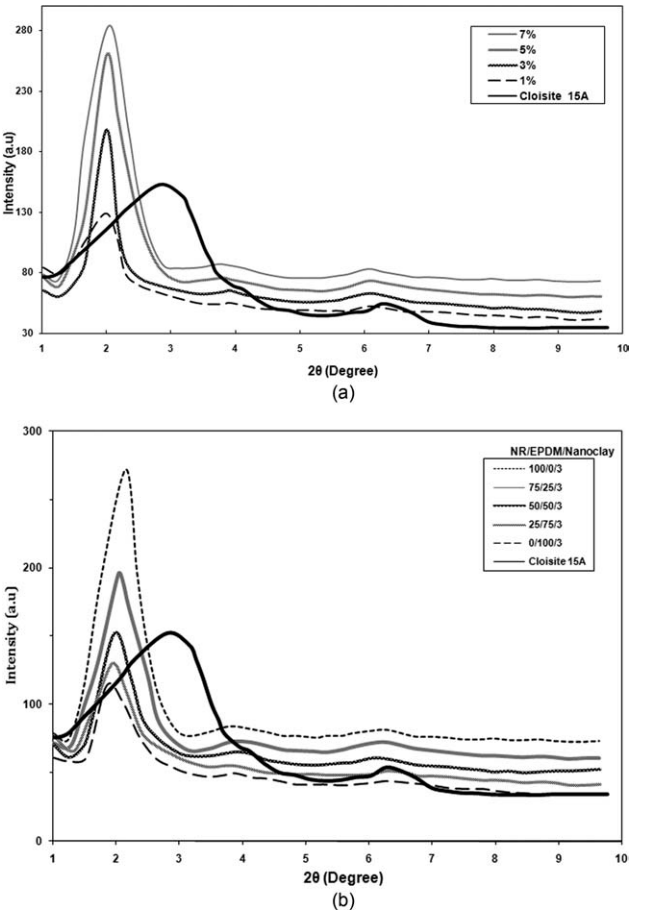

Figure 1. (a) XRD results of NR75/EPDM25 nanocomposites containing 1, 3, 5, and 7 wt % nanoclay. (b) XRD results of different compositions of NR/EPDM containing 3 wt % nanoclay.

and reduction of the peak intensity. It is because of the higher Mooney viscosity of compound resulting in a higher shear stress undergone by the matrix that might help the deagglomeration of the clay stocks within the matrix.[4]

TEM Results

Figure 2 shows the TEM images of cryogenically fractured surfaces of 75NR/25EPDM/3Clay samples in which dark lines represent the Cloisite layers dispersed within the matrix. Light regions depict the phase with lower density (EPDM) and darker regions are representatives of the denser phase (NR) (Table I). Different magnifications of the micrographs imply the intercalation and partial exfoliation of the clay through the polymer matrix, evidenced by XRD patterns.

Swelling Behavior

Table IV presents the solubility and the swelling percentage for the compounds. As seen in Table IV, the unfilled NR/EPDM had the greatest swelling percentage. Addition of the compositions with nanoclay decreases the percentage swelling. This indicates a higher level of effective crosslinks either by interaction between the polymer chains and the filler or by an increased crosslink density due to the addition of nanoparticles.

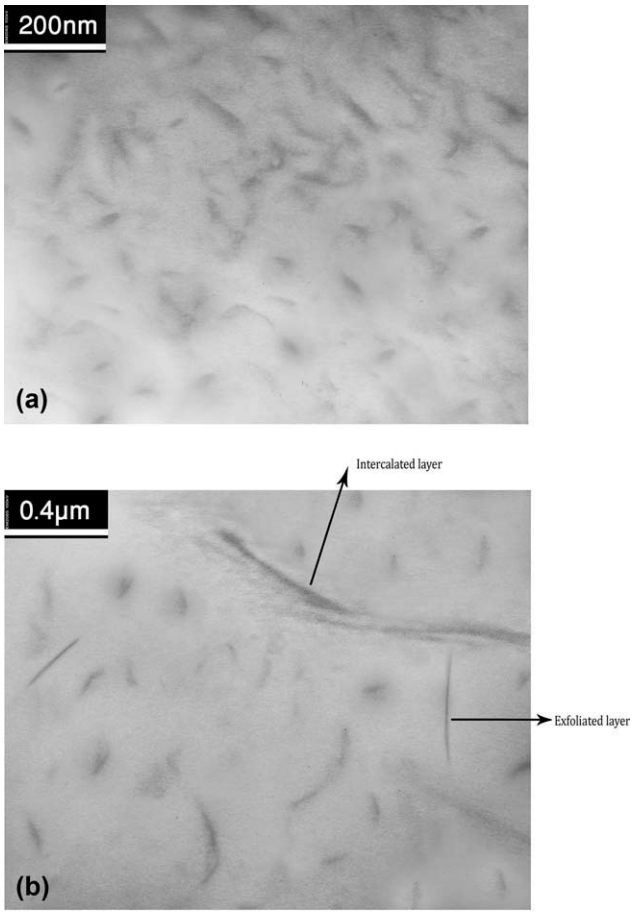

Figure 2. (a) TEM image of NR75/EPDM 25/nanoclay 3. (b) TEM image of NR75/EPDM25/nanoclay 3.

Therefore, NR/EPDM nanocomposites with organoclay absorb less solvent.

Mechanical Properties

The incorporation of organic silicate gives rise to a noticeable increase in mechanical strength which shows the strong reinforcing effect of the inorganic fillers. Table V lists the mechanical properties of NR/EPDM and their composites before and after heat aging in air. As seen in Table V, tensile and compression strength, tensile modulus as well as tear strength of samples are improved by clay loading. The improvements of mechanical strength in case of polymer–clay nanocomposites were given by some researchers.[4,7–9] Their studies suggested that the increase of strength is related to the degree of dispersion of clay layers into the polymer matrix. Some explanations were presented on the basis of interfacial properties and restricted mobility of the polymer chain. Improved mechanical strength is an indirect measure of good interactions established between clay and matrix. The reinforcement is also associated with the anisotropy and high aspect ratio of organoclay nanofillers, which act as short reinforcing fibers with nanoscale architecture. Clay with high aspect ratio is more efficient in restricting the rubber chains and in resisting the development of cracks than spherical fillers. In a fixed clay content, as the NR content of the samples increases, both tensile and tear strength increase,

Table IV. Percentage Swelling for NR/EPDM Samples with and Without Nanoclay

Composition (NR/EPDM/Nanoclay)	Swelling (%)	Solubility (%)
75/25/0	320 ± 20	6.29 ± 0.37
75/25/1	295 ± 20	5.34 ± 0.23
75/25/3	280 ± 15	4.53 ± 0.17
75/25/5	250 ± 16	3.87 ± 0.23
75/25/7	237 ± 15	3.01 ± 0.02

but the compression strength and tensile modulus decreases. On the other hand, the mechanical properties of NR rich vulcanizates decreased dramatically after the aging time. However, EPDM rich vulcanizates possessed thermally stable mechanical strength. The NR rich blends were affected more by the aging time than the EPDM rich blends, as expected. Mechanical properties of NR rich vulcanizates highly decreased with thermal aging. However, EPDM rich vulcanizate showed more thermal stability because of the low diene content of EPDM. Furthermore, addition of nanoclay particles leads to thermal stability of samples. Clay platelets, hindering the thermally caused defects into the polymer bulk would increase the aging resistance of nanocomposites. The studies on the improvement of aging resistance and thermal stability by polymer–clay nanocomposites have been extensively reported.[25–27] Generally, the incorporation of clay into the polymer matrix is found to enhance thermal

Table V. Mechanical Properties of Prepared Samples Before and After Thermal Aging

Sample code (Dimensions)	Tensile strength (MPa)	Compression strength (MPa)	Tear strength (MPa)	Modulus 100% (MPa)
Before aging				
S_0	1.403	0.72	18.1	0.90
S_1	5.3	0.9	19.64	1.07
S_2	8.247	0.93	21.1	1.09
S_3	10.12	0.957	22.8	1.14
S_4	10.795	0.998	24.75	1.26
S_5	18.5	1.02	28.59	1.09
S_6	4.4	1.068	19.3	1.10
S_7	3.89	1.075	18.8	1.17
S_8	1.59	1.078	16.2	1.20
After aging				
S_0	0.98	0.50	12.67	0.63
S_1	3.975	0.68	14.74	0.80
S_2	6.43	0.72	18.568	0.85
S_3	8.19	0.765	18.24	0.91
S_4	9.17	0.867	21.03	1.07
S_5	12.395	0.67	18.68	0.7
S_6	3.82	0.91	16.598	0.95
S_7	3.42	0.96	16.92	1.05
S_8	1.43	1.01	14.74	1.1

Applied Polymer SCIENCE

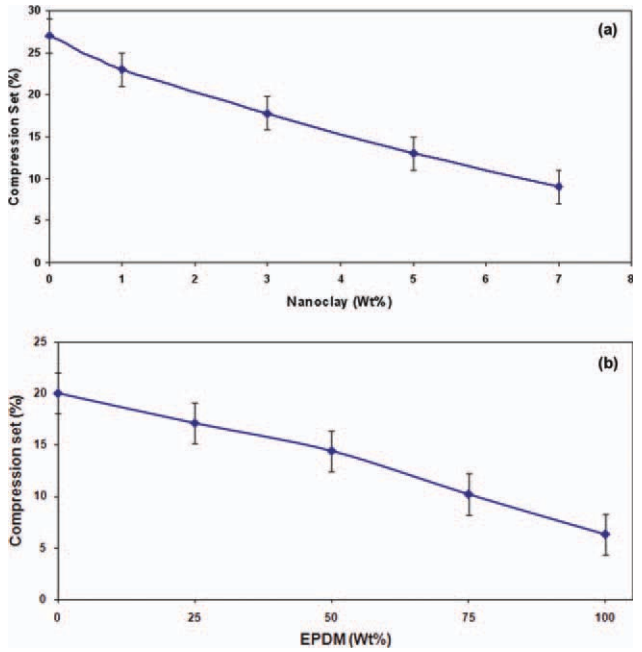

Figure 3. (a) Compression set results of NR/EPDM (75/25). (b) Compression set results of different compositions of NR/EPDM containing 3 wt % nanoclay. [Color figure can be viewed in the online issue, which is available at wileyonlinelibrary.com.]

stability by acting as a superior insulator and mass transport barrier to the volatile products generated during decomposition.

Compression Set Test

Compression set testing measures the ability of the rubber to return to its original thickness after prolonged compressive stresses at a given temperature and deflection. As a rubber material is compressed over time, it loses its ability to return to its original thickness. The results of the compression set for the NR/EPDM (75/25) samples containing 1, 3, 5, and 7 wt % nanoclay and different compositions of NR/EPDM containing 3 wt % nanoclay are shown in Figure 3. Inserting the organoclay in the rubber matrix greatly reduces the deformation sustained by the elastomer [Figure 3(a)]. The poor performance of materials in terms of compression set is attributed to uncrosslinked chains and to network defects such as long dangling chains, which do not contribute to the permanent network and are able to relax during the compression stage, then providing no elastic contribution to the recovery stage.[28] In NR/EPDM samples, the nanoclay results in restriction in polymer chain movements and lower compression set. Other researchers have reported that increased formation of effective network chains or crosslinking in the deformed state decreases compression set. Furthermore, they could show that the smaller the size of particles the lower the compression set could become.[29,30] Therefore, addition of nanoclay in this study with resultant reduced compression set indicates such effects reported by previous researchers. Furthermore, Figure 3(b) shows the results of compression set of different compositions of NR/EPDM containing 3 wt % nanoclay. As seen the compression set decreases as the EPDM content increases in the blend.

Dynamic Properties

To make a complete exploration of the advantages offered by the nanoclay in NR/EPDM rubber compounds, we looked also at certain dynamic properties such as the generation of heat under cyclic deformation. We have used the classic test of the Goodrich flexometer and the temperature increase was then divided by the hardness of the sample to have a heat index (Figure 4). It can be observed that the heat build up decreases by adding the nanoclay. Thus, the nanoclay offers also the beneficial effect of being able to reduce the hysteresis of a rubber compound. Similar trend was observed by Cataldo.[31]

Investigation into Stress–Strain Behavior by Hyperelastic Models

Figure 5 shows the geometry of the samples as well as the boundary condition. Material constants of the mentioned models are listed in Tables VI and VII. Insights on the stress–strain behavior of the prepared samples by using hyperelastic models are illustrated in Figures 6 and 7. Before discussing about the applicability of the hyperelastic models, it is worth interpreting the stress–strain curves of the samples. As seen in Figure 6, the tensile strength, modulus, and compression strength of NR/EPDM(75/25) improved by increasing the clay content attributing this improvement to the state of intercalation/exfoliation of the nanocomposite and also the confinement of polymer chains arising from the presence of clay in the matrix.[4] Stress-induced orientation of Clay layers under the tensile stress results in a considerable increase in the tensile properties of intercalated/exfoliated nanocomposites.[4] The uncommon increase observed in the elongation at break with nanoclay content is ascribed to the fact that some rubber chains are not crosslinked with sulfur in the presence of silicate layers; these uncrosslinked chains are responsible for the increment in elongation of nanocomposite

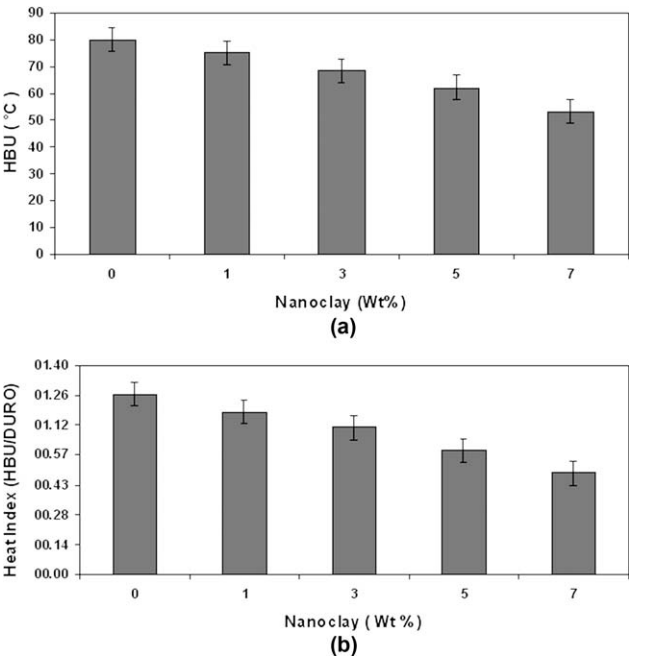

Figure 4. (a) Value of heat build up for NR/EPDM (75/25) nanocomposites. (b) Value of heat index for NR/EPDM (75/25) nanocomposites.

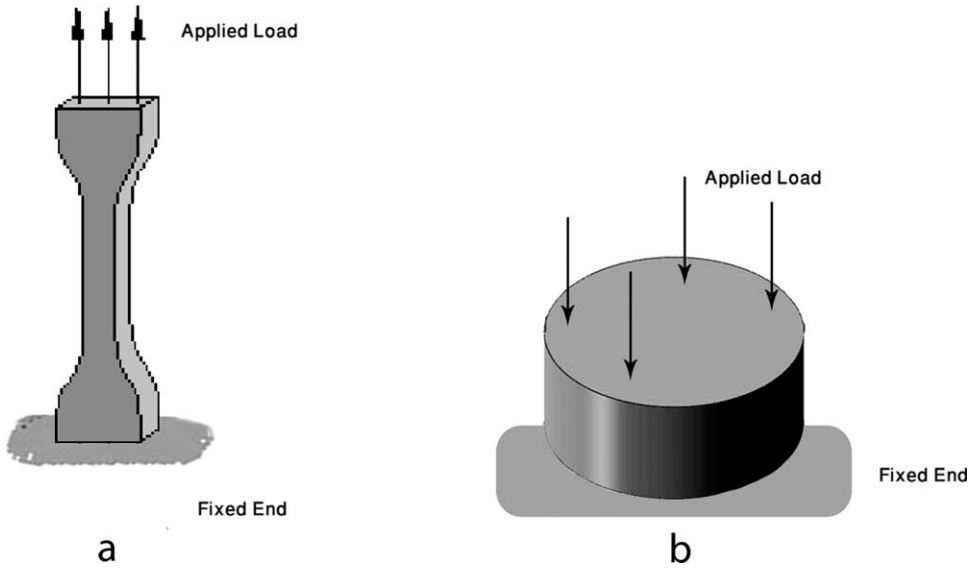

Figure 5. Sample geometry with the boundary conditions for (a) tension test (b) compression test.

samples at break. This phenomenon has been also reported by other researchers.[4] On the other hand, from Figure 7, it is seen that in a fixed clay content, decreasing EPDM results in an increase in the tensile strength of the samples and reducing the compression strength. The downfall of elongation at break with EPDM is the result of lower elasticity of EPDM compared with NR. These trends were reported by Alipour et al.[4]

In Figure 6, nominal stress versus nominal strain values obtained from experimental data and data predicted by five hyperelastic models for NR/EPDM (75/25) nanocomposite samples containing 0, 1, 3, 5, and 7 wt % nanoclay are reported. As seen in compression state, the agreement between experimental data and theoretical calculations for the third order Ogden, second order Polynomial, Marlow, and Yeoh does not change with nanoclay content. A different trend is observed for Arruda-Boyce model, a reasonable agreement between experimental and theoretical calculations can be observed when nanoclay content in samples increases. In tension states, in zero and small strains, the third order Ogden, second order Polynomial and Marlow models can accurately fit the experimental data while the Arruda-Boyce and Yeoh models show some degree of deviation from actual data when the nanoclay content of samples decreases.

It should be noted that in middle strains, the agreement between theoretical calculations and experiments is still quite acceptable for the third order Ogden, second order Polynomial and Marlow models and degree of fitting for these models does not change with nanoclay content. In middle strains, theoretical calculations predicted by the Arruda-Boyce and Yeoh models have more deviation from experiments as nanoclay content of the samples decreases. In larger strains, the applicability of the third order Ogden, second order Polynomial and Marlow models does not alter and they show an excellent agreement for all samples. It means despite the formation of nanostructure in rubber compounds, applicability of these models does not change and they show an acceptable fit for all samples. On the other hand, the Arruda-Boyce and Yeoh models just give reasonable degree of agreements between real and computed data when nanoclay content of the samples increases and the degree of fitting for the samples containing 0 and 1 wt % nanoclay is not satisfactory.

Table VI. Material Parameters of Arruda-Boyce and the Third Order Ogden Models for Prepared Samples

	Arruda-Boyce			Ogden 3					
Sample	μ	μ_0	λ_m	μ_1	μ_2	μ_3	α_1	α_2	α_3
S_0	0.78098	0.78098	3371.34	−24.52799	10.93983	14.33905	0.786171	1.320987	0.21769
S_1	0.73195	0.76803	3.62257	8.35E-02	1.55E-05	0.692221	3.593286	9.749567	−3.9064
S_2	0.44251	0.48046	2.81909	−14.56058	1.29E-06	14.89744	−2.989092	11.25523	−3.3512
S_3	0.65651	0.69725	3.25868	2.69E-02	2.32E-05	0.628209	2.245507	9.32372	−5.8543
S_4	0.46461	0.50402	2.83307	−13.88589	1.06E-06	14.22878	−2.850278	11.32321	−3.2948
S_5	0.61699	0.6619	3.03241	0.124337	2.02E-05	0.47759	2.478808	9.473801	−6.1527
S_6	0.99581	0.99581	5152.54	−1.54	5.56E-02	2.57785	0.667099	4.618985	−5E-06
S_7	0.76591	0.76591	2216.99	−3.082934	1.32E-03	3.81827	−2.583361	6.586752	−3.1071
S_8	0.97614	0.97614	4331.35	−27.60189	1.28E+01	15.804	−0.139	0.439282	−0.7514

Table VII. Material Parameters of Yeoh and the Second Order Polynomial Models for Prepared Samples

	Yeoh			Polynomial ($N = 2$)				
Sample	C1	C20	C30	C10	C20	C01	C11	C02
S_0	0.42063	−1.33E-01	6.95E-03	−1.85E-03	−0.13302	0.43179	0.556288	−0.5313
S_1	0.4268	4.15E-03	7.96E-04	0.609137	4.15E-03	7.51E-02	0.131045	−0.5382
S_2	0.23758	2.61E-03	3.02E-04	0.592388	4.02E-02	1.71E-02	−1.71E-03	−0.1639
S_3	0.38292	2.08E-02	5.78E-04	0.702772	2.80E-02	1.36E-02	1.36E-03	−0.3701
S_4	0.24622	4.33E-03	2.53E-04	0.58106	4.04E-02	6.58E-02	6.58E-02	−0.1339
S_5	0.34975	−5.76E-03	5.62E-04	0.97421	4.99E-02	−0.25827	−0.10803	−0.3359
S_6	0.56863	−3.41E-02	1.62E-03	0.393088	−1.71E-03	2.75E-01	1.35E-01	0.13544
S_7	0.42158	−1.73E-02	6.36E-04	0.446527	−1.77E-03	0.24648	0.21514	0.21514
S_8	0.54836	−5.29E-02	3.89E-03	0.133258	−9.75E-02	0.48702	0.471746	−0.5649

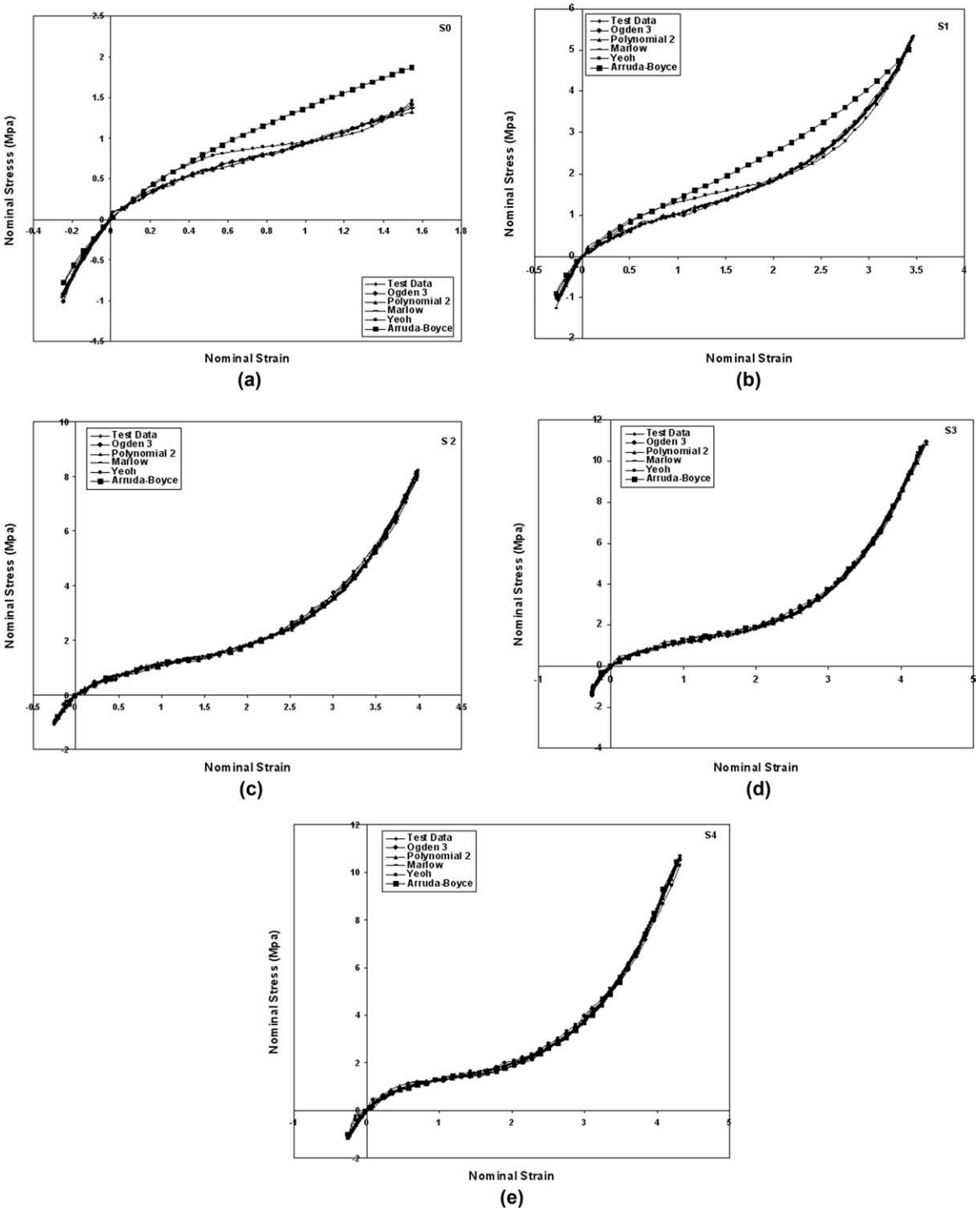

Figure 6. (a) Nominal stress-nominal strain curve for sample S_0. (b) Nominal stress-nominal strain curve for sample S_1. (c) Nominal stress-nominal strain curve for sample S_2. (d) Nominal stress-nominal strain curve for sample S_3. (e) Nominal stress-nominal strain curve for sample S_4.

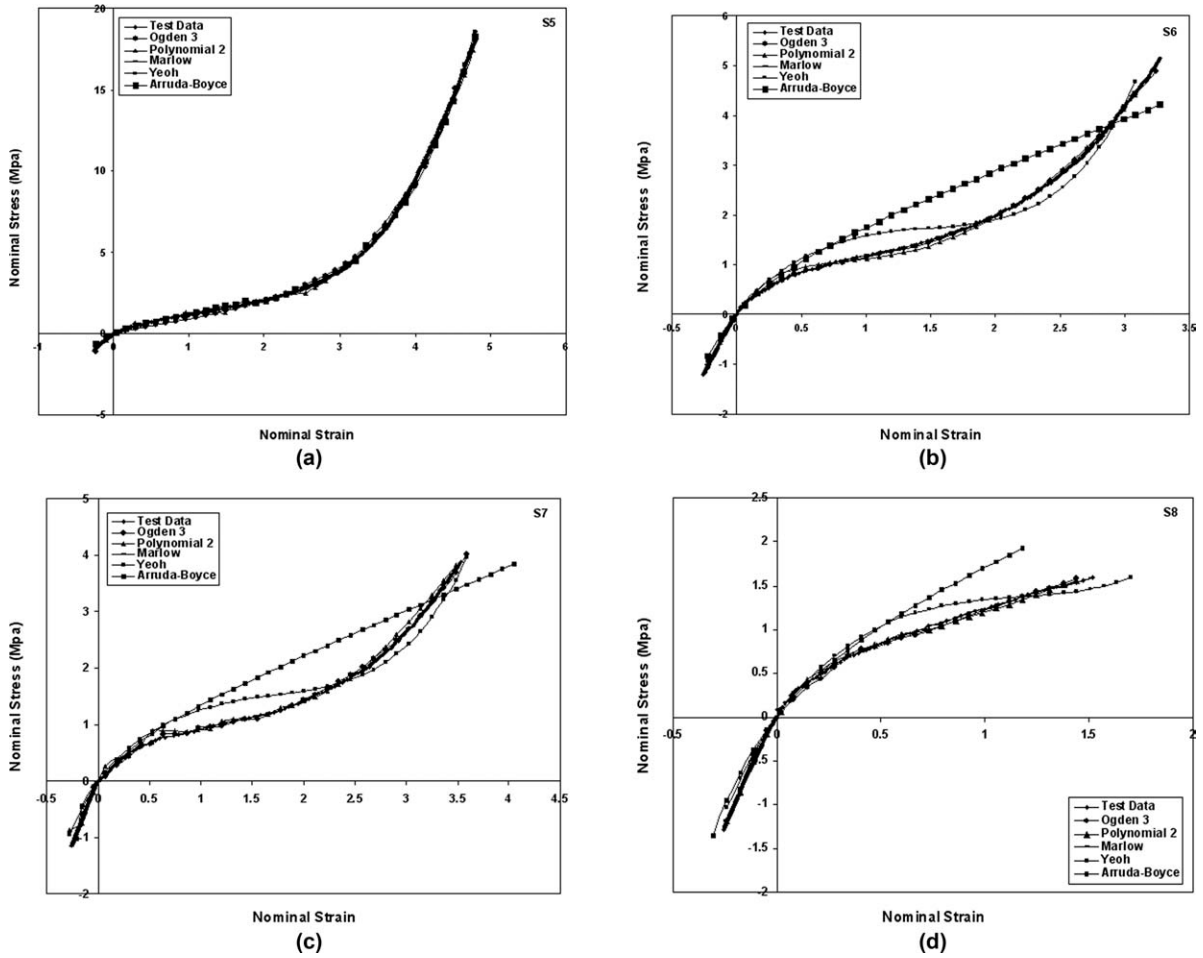

Figure 7. (a) Nominal stress-nominal strain curve for sample S_5. (b) Nominal stress-nominal strain curve for sample S_6. (c) Nominal stress-nominal strain curve for sample S_7. (d) Nominal stress-nominal strain curve for sample S_8.

According to the obtained results, it can be pointed that the applicability of Arruda-Boyce model and Yeoh model depends on the content of nanoclay. In higher amount of nanoclay (3, 5, and 7%) which the interaction established between polymer/nanoparticles is much more, these models show a good agreement with experiments. In Arruda-Boyce model, underlying molecular structure of the elastomer represents the physics of network deformation and is represented to simulate the non-Gaussian behavior of individual chains in the network.[20] As nanoclay content of the samples reduces, the behavior of polymeric chains in the nanostructured compound does not consent to non-Gaussian and consequently, inconsistency between experimental data and model predictions are noticed.

To probe the effect of rubber composition on the applicability of above mentioned models, nominal stress versus nominal strain obtained from experimental and model predictions for NR/EPDM nanocomposites with different matrix compositions including 0/100, 25/75, 50/50, 75/25, and 100/0 containing 3 wt % of Cloisite 15A are illustrated in Figure 7. In negative region, the inconsistency between experimental data and those predicted by Arruda-Boyce and Yeoh models could be observed when the EPDM content of samples increases while other models can completely fit the experimental data without any deviation. In zero and small strains nearly all hyperleastic models have acceptable degree of fitting with care since the theoretical calculations predicted by Arruda-Boyce and Yeoh models are not as accurate as those predicted by other models and these two models show deviation to some extent with the increase in EPDM content of samples. In middle and large strains, an excellent degree of fitting can be observed by the third order Ogden, second order Polynomial and Marlow models in all matrix compositions. On the other hand, predicted data by Arruda-Boyce and Yeoh models show disagreement with experimental data in middle and large strains as the EPDM content of the samples increases. The inconsistency between experimental and predicted data by Arruda-Boyce model might be as a consequence of the changes of molecular orientation in such a way that they do not comply with the basic assumption of this model.[21]

So, according to the obtained results, it can be expressed that the third order Ogden, second order Polynomial and Marlow models can truly predict stress–strain behavior of nanocomposite samples in all strain regions, both in tension and compression states at different nanoclay loading and rubber compositions with a high degree of accuracy. On the contrary, Arruda-

Boyce and Yeoh cannot predict the true behavior of samples in all strain regions for all clay loadings and matrix compositions. In conclusion, decrease of nanoclay content or increase of EPDM content changes the dynamic of the macromolecular motions in such a way that it reveals the necessity of new investigations to evolve new models for depiction of the mechanical treatment of the elastomer nanocomposites.

CONCLUSIONS

This work was devoted to investigate the rubber composition and nanoclay content on the properties and the stress–strain behavior of NR/EPDM/Cloisite 15A nanocomposites using different constitutive models. Base on the results of this work, the following conclusions can be drawn as follows:

1. Experimental results of X-ray diffraction showed expansion of the distance between the silicate layers and transmission electron microscopy (TEM) proved that the silicate layers existed in the form of an intercalated and partially exfoliated layer structure.
2. In comparison with pure NR/EPDM, mechanical properties of the resulting nanocomposites receive markedly increases by clay loading.
3. The more EPDM content, the more tensile modulus, compression strength, compression set, and thermal stability would become.
4. It was shown that matrix composition and nanoclay content have a great effect on the degree of agreement between experimental data and those predicted by hyperelastic models. The third order Ogden, second order Polynomial and Marlow models are able to predict the true behavior of the samples at various amounts of nanoclay and different matrix compositions, both in tension and compression states, in all regions of the stress–strain curve of the samples. It was concluded that Arruda-Boyce and Yeoh models should be used with care since they have more deviation from experimental data as nanoclay content decreases or EPDM content of samples increases. It should be noted that Arruda-Boyce and Yeoh models just show a reasonable degree of fitting in compression state and in small strains when clay content increases and EPDM content decreases.

ACKNOWLEDGMENTS

The financial support by Iran Nanotechnology Initiative Council is gratefully acknowledged by the authors. The authors also thank Islamic Azad University, Zarghan branch for supporting this research.

REFERENCES

1. Bhowmick, A. K.; Chakraborty, B. *Plast. Rubber Process. Appl.* **1989,** *11*, 99.
2. Costa, V. G.; Nunes, R. C. R. *Eur. Polym. J.* **1994,** *30*, 1025.
3. Cheremisinoff, N. P. *Polym. Plast. Technol. Eng.* **1992,** *31*, 713.
4. Alipour, A.; Naderi, G.; Bakhshandeh, G. R.; Vali, H.; Shokoohi, Sh. *Int. Polym. Proc.* **2011,** *XXVI*, 48.
5. Naderi, G.; Lafleur, P. G.; Dubois, C. *Polym. Compos.* **2008,** *29*, 1301.
6. Naderi, G.; Lafleur, P. G.; Dubois, C. *Polym. Eng. Sci.* **2007,** *47*, 207.
7. Varghese, S.; Gatos, K.; Apostolov, A.; Karger-Kocsis, J. *J. Appl. Polym. Sci.* **2004,** *92*, 543.
8. Bala, P.; Samantaray, B. K.; Srivastava, S. K. *J. Appl. Polym. Sci.* **2004,** *92*, 3853.
9. Lopez-Manchado, M. A.; Herrero, B.; Arroyo, M. *Polym. Int.* **2004,** *53*, 1766.
10. Morman, K. N.; Pan, T. Y. *Rubber Chem. Technol.* **1998,** *61*, 503.
11. Nicholson, D. W.; Nelson, W. N.; Lin, B.; Farinella, A. *Appl. Mech. Rev.* **1990,** *51*, 303.
12. Nicholson, D. W.; Nelson, W. N. *Rubber Chem. Technol.* **1998,** *63*, 368.
13. Muhr, A. H. *Rubber Chem. Technol.* **2005,** *78*, 391.
14. Beda, T. *J. Polym. Sci. Part B: Polym. Phys.* **2007,** *45*, 1713.
15. Finney, R. H.; Kumar, A. *Rubber Chem. Technol.* **1988,** *61*, 879.
16. Li-Rong, W.; Zhen-Hua, L. *Rubber Chem. Technol.* **2003,** *76*, 271.
17. Yeoh, O. H. *Rubber Chem. Technol.* **1993,** *66*, 754.
18. Arruda, E. M.; Boyce, M. C. *J. Mech. Phys. Solids* **1993,** *41*, 398.
19. Ogden, R. W. *Rubber Chem. Technol.* **1986,** *59*, 361.
20. Ghoreishy, M. H. R. *Iranian Rubber Mag.* **2008,** *13*, 4.
21. Ghasemi, I.; Karrabi, M.; Ghoreishy, M. H. R. *Plast. Rubber Compos.* **2008,** *37*, 305.
22. Ghoreishy, M. H. R. *J. Mater. Design.* **2012,** *35*, 791.
23. Ghoreishy, M. H. R. *Iranian J. Polym. Sci. Technol.* **2009,** *23*, 273.
24. ABAQUS 2008, version 6.8.
25. Blumstein, A. *J. Polym. Sci. Part A: Gen. Pap.* **1965,** *3*, 2665.
26. Burnside, S. D.; Giannelis, E. P. *Chem. Mater.* **1995,** *7*, 1597.
27. Wang, S. J.; Long, C. F.; Wang, X. Y. *J. Appl. Polym. Sci.* **1998,** *69*, 1557.
28. Martin, G.; Barre, C.; Cassagnau, P.; Sonntag, P.; Garois, N. *Polymer* **1982,** *49*, e1892.
29. Hao, P. T.; Ismail, H.; Hashim, A. S. In Paper Presented at the 3rd Regional IMT–GT Ininet Conference; Medan, Indonesia, **2000.**
30. Jalham, I. S.; Maita, I. J. *J. Compos. Mater.* **2006,** *40*, 2099.
31. Cataldo, F. *Macromol. Symp.* **2007,** *247*, 67.
32. Maiti, M.; Bhowmick, A. K. *J. Polym. Sci.* **2006,** *44*, 162.